

# Development of a Cold Plate for Spatial and Temporal Temperature Uniformity

Michael C. Ellis<sup>1</sup>, Elizabeth K. Seber<sup>2</sup> and George Elias<sup>3</sup>  
*Advanced Cooling Technologies, Inc., Lancaster, PA, 17601*

Electronics instrumentation, such as those used in low-orbit for monitoring environmental change, are very sensitive to temperature change. Such instrumentation should be maintained at a consistent temperature despite changing radiator/condenser temperatures. Such a thermal system must also be low in size, weight, and power. Advanced Cooling Technologies, Inc. (ACT) has developed a cold plate which, through variable thermal conductance, provides spatial and temporal temperature uniformity to address this need. The technology builds on ACT's experience with passive two-phase devices, specifically variable conductance heat pipes (VCHP) and vapor chambers. Isothermality is handled by the VCHPs, which are charged with a working fluid at saturation conditions and a non-condensable gas (NCG). During operation, vapor that is generated from the evaporator end moves to the condenser end. As the heat load or as the sink temperature increases, the working fluid will seek to operate at a higher temperature. This results in increased pressure as the working fluid exists at saturation conditions. This increase pushes back the NCG and opens up more condensing area. As the opposite occurs, the NCG pushes forward and blankets a portion of the condensing area of the VCHP. As a result of the changing condenser surface area, the conductance of the heat pipe is variable, which allows the VCHP to carry heat at a higher rate and mitigate the effects of heat load or sink temperature changes. During a NASA Phase I SBIR, ACT has developed and fabricated a subscale prototype Variable Conductance Cold Plate (VCCP). During testing, ACT demonstrated the cold plate surface temporal temperature change of less than 0.05 K/min. As a part of the Phase II SBIR, ACT is expanding on this technology to develop a VCCP with a heat-collection surface of 0.5 m<sup>2</sup> in size. ACT is also currently investigating future missions for which the design can be tailored.

## Nomenclature

$A$	=	Area
CCHP	=	Constant Conductance Heat Pipe
$dx$	=	thickness
$d_{wire}$	=	Wire Diameter
$\Delta P$	=	Pressure Drop
$\Delta T$	=	Temperature Difference
$\epsilon_{wick}$	=	Wick Porosity
$g$	=	Gravity
$h_{fg}$	=	Latent Heat of Vaporization
$H_{chamber}$	=	Chamber Height
$k$	=	Thermal Conductivity
$K_{wick}$	=	Wick Permeability
$\mu$	=	Liquid Viscosity
$n$	=	Number of Moles
NCG	=	Non-Condensable Gas
$N_{mesh}$	=	Number of Screen-Wick Wraps
$P$	=	Pressure

---

<sup>1</sup> Senior Engineer, R&D, 1046 New Holland Avenue, Lancaster, PA 17601, USA.

<sup>2</sup> R&D Engineer I, R&D, 1046 New Holland Avenue, Lancaster, PA 17601, USA.

<sup>3</sup> R&D Engineer I, R&D, 1046 New Holland Avenue, Lancaster, PA 17601, USA.

$\dot{Q}$	=	Heat Transfer Rate
$r_c$	=	Wick Pore Radius
$R$	=	Thermal Resistance
$\rho$	=	Liquid Density
$s_{wire}$	=	Wire Spacing
$\sigma$	=	Surface Tension
$T$	=	Temperature
$\theta$	=	Contact Angle
$V$	=	Volume
$\dot{V}$	=	Volumetric Flow Rate
VCCP	=	Variable Conductance Cold Plate
VCHP	=	Variable Conductance Heat Pipe

## I. Introduction

**T**WO-PHASE thermal management systems have several advantages over single-phase systems at significant heat loads. Primarily, they provide equivalent thermal management capacity with reduced mass, volume, and power usage while providing performance improvements such as enhanced heat transfer and temperature uniformity. The concept discussed here builds on the well-known spatial temperature stability associated with two-phase heat transfer by relying on the unique behavior of a fluid at the saturation state to provide temporal temperature stability as well. ACT has designed a Variable Conductance Cold Plate (VCCP) that is capable of significant power rejection while maintaining low spatial and temporal temperature deviation. Electronics instrumentation, such as that used in low-orbit for monitoring environmental changes, are very sensitive to temperature change. Such instrumentation performs best when held at a consistent temperature, despite changing power load and sink conditions. The VCCP concept is intended to provide this capability and relies on three main technologies: a vapor chamber, Variable Conductance Heat Pipes (VCHPs), and a two-phase heat exchanger, as shown in Figure 1. Electronics and instrumentation are mounted to the heat collection surface of the vapor chamber. Inside the vapor chamber, a working fluid exists at saturation with liquid occupying a wick structure that is located along the entire inner surface and allows for evaporation at the heat collection surface and liquid return from the liquid rejection surface. Vapor occupies the remaining space between these surfaces. As heat is generated by the devices mounted on the heat collection surface, liquid in the wick evaporates. This can occur at multiple locations across the surface. The heated vapor then condenses on the heat rejection surface, which in this cold plate design is the exterior of the VCHP evaporator. This condensed liquid is then wicked back to the heat collection surface via capillary pressure. In this way, a vapor chamber can transport heat from a large surface with arbitrary heat source locations to the VCHPs, which then transport this heat to the ultimate sink. Since this heat is transported as latent heat, the entire process is nearly isothermal. This is the purpose of the vapor chamber: to provide spatial isothermality for multiple heat sources in arbitrary locations.

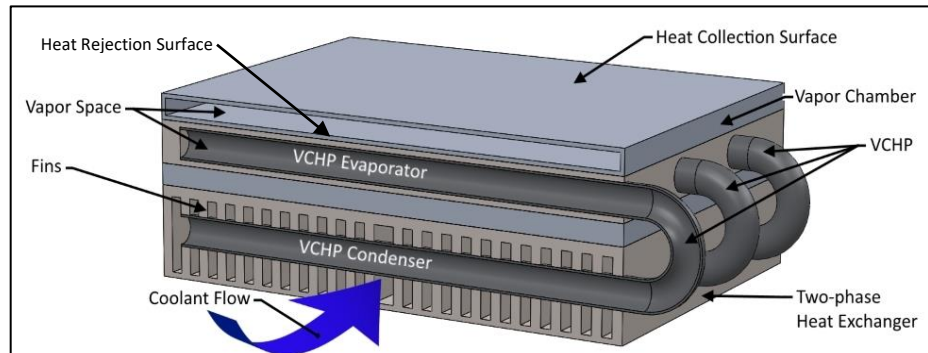


**Figure 1. Cold Plate Concept. Components are oversized and the design simplified to aid in visualization.**

As heat is generated by the devices mounted on the heat collection surface, liquid in the wick evaporates. This can occur at multiple locations across the surface. The heated vapor then condenses on the heat rejection surface, which in this cold plate design is the exterior of the VCHP evaporator. This condensed liquid is then wicked back to the heat collection surface via capillary pressure. In this way, a vapor chamber can transport heat from a large surface with arbitrary heat source locations to the VCHPs, which then transport this heat to the ultimate sink. Since this heat is transported as latent heat, the entire process is nearly isothermal. This is the purpose of the vapor chamber: to provide spatial isothermality for multiple heat sources in arbitrary locations.

Temporal isothermality is then achieved by the VCHPs, which are heat pipes charged with a working fluid at saturation condition and a non-condensable gas (NCG). During operation, vapor generated in the heat pipe's evaporator moves to the condenser, and liquid that forms in the condenser moves back to the evaporator through wicks in the same manner as described previously for the vapor chamber. Vapor in the VCHP continuously pushes the NCG to the far end of the condenser and forms a pocket of NCG that reduces the available condensing area. Typically, an extra volume is allotted beyond the condenser for NCG collection and is known as the NCG reservoir. The length of this pocket in the condenser depends on the balance between the vapor pressure of the working fluid and the NCG mass with which the VCHP is charged.

As the heat load from the vapor chamber increases, or as the sink temperature increases, the working fluid and NCG will seek to operate at a higher temperature. This will result in an increase in the vapor pressure of the saturated fluid and partial pressure of the NCG. The relationship between the rates of change of pressure with respect to temperature of these two substances is important for proper VCHP operation. The NCG rate of change depends on the amount present, which is controlled to a specific mass during charging, and is relatively constant for a monoatomic gas like Argon. The working fluid rate of change in vapor pressure depends on the saturation curve and increases more and more rapidly as fluid temperature increases from the triple point to the critical point. As a result, there is an inflection temperature about which the rate of change of the working fluid pressure is either greater or less than that of the NCG. Above this temperature, an increase in heat load or sink temperature will result in an expansion of the working fluid volume and contraction of the NCG volume. This increases the available condensation area and suppresses the effect of increasing heat load or sink temperature.

Operating on the other end of the temperature range will cause the opposite to occur. In effect, the VCHP condensing area will decrease with increasing temperature and accelerate temperature increase of the working fluid. As this mode of operation is undesirable, care must be taken during design to ensure the VCHP operates in the correct range. For a properly designed VCHP, large changes in the condensing area are possible with very small changes in working fluid temperature. This feature allows the VCHP to provide low rates of temperature change, in other words, maintain temperature isothermality, despite relatively rapid heat load or sink temperature changes.

The variable thermal resistance feature of VCHPs has an additional benefit for spacecraft thermal management. Since the thermal resistance of the cold plate continues to increase as temperature decreases, the temperature difference between the cold plate surface and ultimate heat sink also continues to increase. Eventually, a VCHP can completely shut down and prevent any heat transport. Without this feature, the cold plate surface would eventually reach the ultimate sink temperature after long exposure periods, which can be common for spacecraft. Exposing spacecraft electronics to these temperatures, which can be as cold as the lowest energies that exist in space, is undesirable. The VCHP will not only provide a buffer between the electronics and these cold temperatures but will stop removing heat from the cold plate once the freezing point of the working fluid is reached. Furthermore, since the NCG will expand as the VCHP gets colder, the working fluid will freeze in the evaporator. By including a wick in the evaporator, damage to the VCHP can be prevented and the VCHP will restart without issue once sufficient heat is available to melt the working fluid.

Finally, the heat transported by the vapor chamber and VCHPs is rejected to a two-phase heat exchanger. This heat exchanger will allow for the transfer of latent heat between the VCHP condensers and the working fluid of the coolant system. This coolant, such as R245fa, will enter the heat exchanger either subcooled or at a low-quality saturation state. For the largest degree of subcooling, the overall heat transfer coefficient of the heat exchanger will be minimal as a significant section of the heat exchanger area will be dedicated to single-phase cooling. In a standard heat pipe, this would result in an increase in working fluid temperature. However, the VCHP will respond to this changing heat transfer rate as described previously and maintain working fluid temperature near the desired operating temperature. For coolant entering at a saturated state, the overall heat transfer coefficient of the heat exchanger will be much higher due to an increase in the heat exchanger area available for two-phase heat transfer. Again, the VCHP will respond by reducing the effective condensing length inside the tube. In effect, the VCHP will adjust the effective heat exchanger length as sink conditions change to maintain the cold plate surface temperature.

Together, these components are capable of providing spatial and temporal isothermality over a large surface area by exploiting passive two-phase flow phenomena. Coupled with the size, mass, and power benefits of a pumped, two-phase heat rejection system, the designed cold plate is a compact, low mass, and low power two-phase thermal management system with a variable conductance cold plate that provides spatial and temporal isothermality.

## II. Analytical Model

### A. Methodology

ACT has developed a system model to predict performance not only as conditions change but also as aspects of the design change. This model includes three major components: the vapor chamber, the VCHP, and the heat exchanger. ACT has developed analytical models of all three of these components in the past, but improved upon previous work by integrating these models to allow for optimization of the system as a whole.

To start, parameters such as heat load and basic geometries of the system are defined. It helps during this portion to also understand what the desired outputs will be. In this model, the most interesting output will be how the temperatures of the cold plate and vapor chamber change with varying sink temperatures. Therefore, the conditions of the sink must be predefined. For now, the model will focus on just one heat pipe as a single cell. This will make coupling groups of heat pipes easier later on in the model.

Starting at the downstream, or sink end of the heat pipe, a thermal resistance network can be made to determine the temperature of the vapor within the heat pipe. This thermal resistance network, depicted in Figure 2, uses the heat transfer coefficient of a cylinder (the heat pipe) in the cross-flow of a single-phase coolant. In this model, the coolant is a 50% ethylene glycol and water mixture, and the Zhukauskas correlation is used to determine the heat transfer coefficient. This correlation is a single-phase correlation developed by the nuclear industry for flow across banks of tubes in crossflow. The convective heat transfer coefficient and selected geometry can then be used to find the thermal resistance between the coolant flow and the vapor at the interior of the VCHP. The downstream thermal resistance is made to be a function of the length of the condensing region, since this length changes within a VCHP. Knowing the initial temperature of the coolant and the power load each heat pipe cell must dissipate, it is possible now to derive the vapor temperature for a Constant Conductance Heat Pipe (CCHP). However, a little more work is necessary to determine the vapor temperature for a VCHP. At this point, calculating the change in coolant temperature is also possible. This information will be needed when the model is extended to multiple VCHPs to more accurately reflect the prototype design.

Now that all downstream conditions have been established, the vapor temperature for a VCHP can be determined. A few more parameters must be defined here: the volume of the reservoir, the temperature of the reservoir, the maximum length of the condensing section of the heat pipe, and the maximum temperature of the vapor. The maximum vapor temperature is found using the previously calculated downstream thermal resistance network at the maximum condensing length. The reservoir temperature is influenced by the sink temperature and the vapor temperature. The volume of the reservoir is a predefined geometry. For a VCHP, the active length of the condenser is a function of vapor temperature, sink temperature, and heat load. As the latter two variables are inputs, there is only one unknown variable.

To determine the vapor temperature of the VCHP, a relationship between the NCG and vapor must be established. Monoatomic gases such as Argon are typically used as the NCG and the ideal gas law provides a good approximation of the behavior of this gas. For the vapor phase, NIST saturation tables are used to determine fluid density. The balance between the vapor and gas determines the inactive condenser length and vapor temperature. The key area of interest is in the inactive region of the condenser and the inactive condenser length, as shown in Figure 3. The partial pressure of the working fluid and volume across these regions are functions of vapor and sink temperatures. Whether the vapor temperature is at a maximum or at a lower arbitrary value, the number of moles ( $n$ ) must be the same for all cases between the reservoir and the condenser. Using these considerations, a function that is reliant on the vapor temperature, the sink temperature, and the heat load can be

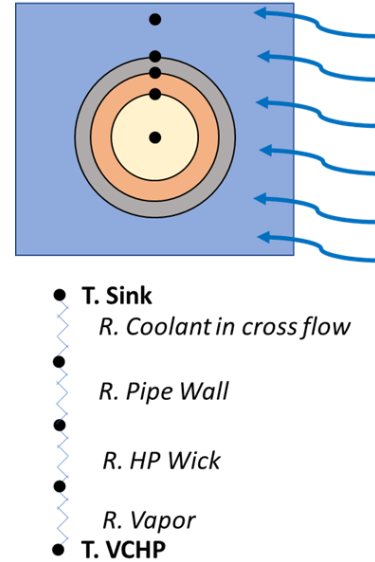
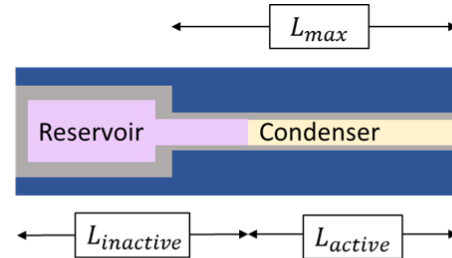


**Figure 2. Thermal Resistance Model of the Heat Sink**



$$n = \frac{P_{\text{partial}} \times V_{\text{inactive}}}{R \times T_{\text{Sink}}}$$

$$F(T_{\text{Sink}}, T_{\text{vapor}}, \text{HeatLoad}) = n(T_{\text{vapormax}}) - n(T_{\text{vapor}})$$

**Figure 3. VCHP Model Concept**

formulated that is the difference between  $n$  at max vapor temperature and  $n$  at an arbitrary vapor temperature. The vapor temperature can then be a function of the root of that difference, where the root function returns a value of vapor temperature that makes that difference zero. As the sink temperature and heat load change, the vapor temperature needed to make that function zero changes as well, thus making the vapor temperature a function of sink temperature and heat load.

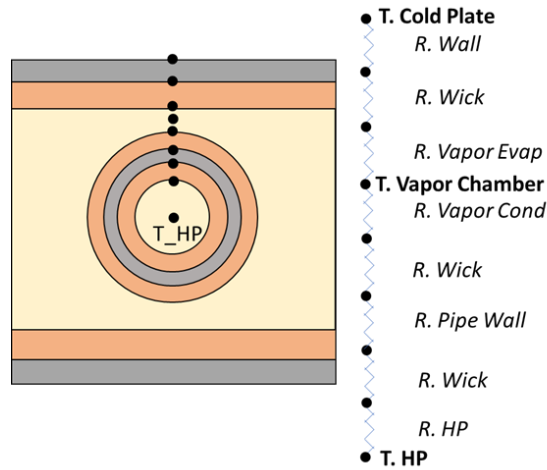


**Figure 4. Evaporator Thermal Resistance Network**

Now that a more accurate vapor temperature can be calculated, determining the temperature of the cold plate and vapor chamber in the upstream (evaporator) section of the heat pipe is very direct. A thermal resistance network, shown in Figure 4, is a straightforward method to determine heat transfer between the vapor of the heat pipe to the vapor of the vapor chamber, and then from the vapor of the vapor chamber to the surface of the cold plate. Using these upstream resistance networks, the two desired output temperatures can be created as functions of heat load and sink temperature. This can also be done with the previously calculated vapor temperature of a CCHP. Figure 5 shows how temperatures at key points throughout similarly sized VCHP and CCHP change with varying coolant temperatures for a given heat load. In this figure, the Heat Pipe Vapor (HP Vapor), the Vapor Chamber Vapor (VC Vapor) and Cold Plate Heat

Collection Surface Temperatures are shown. Note that the temperatures for the cold plate and the vapor chamber change very little in response to changing sink temperatures for the VCHP compared to the change in temperature for the CCHP. It is clear from this graph that the VCHP can hold the cold plate at a much steadier temperature despite fluctuations in conditions in the sink.

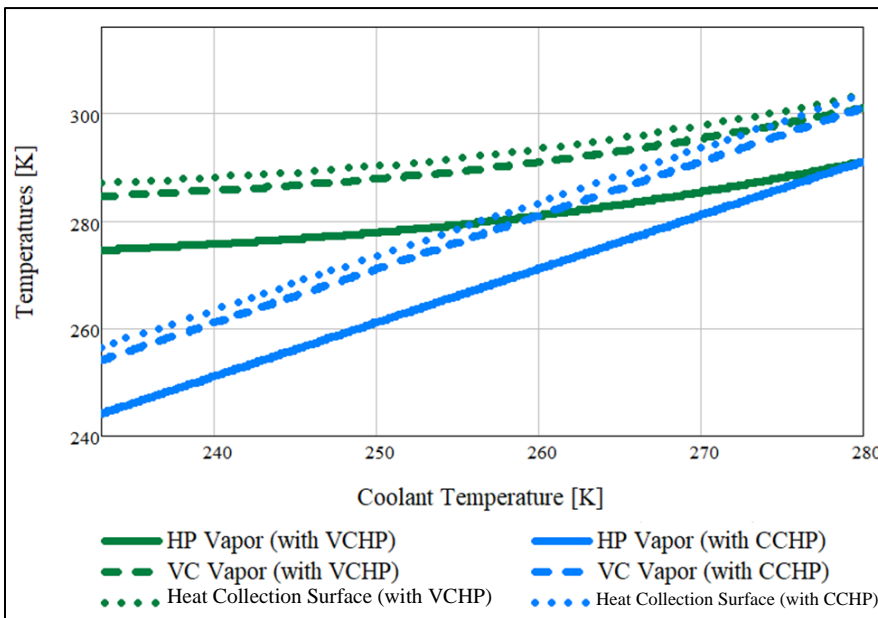


**Figure 5. Relevant Temperature Comparison between designs using VCHPs and CCHPs for varying Sink Temperatures.**

then R245fa, and finally Ammonia. For the purposes of demonstrating proof of concept, acetone was selected as the working fluid. While methanol would analytically perform better, pure methanol is known to attack metals like aluminum and titanium. As such, methanol systems required a copper or stainless-steel envelope, neither of which are known for their lightweight properties. Acetone is compatible with all four of those materials. For these reasons, ACT selected an acetone/aluminum cold plate for the initial subscale prototype. ACT is in the process of using this

**B. Results**

The first study for optimization was to determine the working fluid for the VCCP. Five different working fluids were used as the fluid within the VCHPs: acetone, ammonia, methanol, R245fa and R134fa. For all three cases, acetone was used as the working fluid within the vapor chamber. Out of the fluids tested, methanol had the lowest change in cold plate temperature over the selected range of sink temperatures: 17 K over a 50 K sink temperature change. The results can be seen in Table 1. Acetone performed second best, with a cold plate temperature change of 24 K, and was followed by R134a,

analytical model to design another subscale prototype with ammonia as the working fluid, as ammonia is the preferred choice for spacecraft applications.

**Table 1. Working Fluid Performance Comparison**

Fluid	Temperature Change (K)	Maximum Temperature (K)
Acetone	24	304
Ammonia	37	295
Methanol	17	303
R245fa	32	310
R134a	26	309

The next study focused on changing the nominal diameter of the heat pipes. The five diameters modeled ranged from 0.25 in. to 0.75 in. The thickness of the interior wick remained the same for each case as it is a parameter that will also be optimized later on, although this would also likely change with diameter size. By changing the diameter, other important variables such as thermal coefficients and thermal resistances for each pipe changed. The effects of the varying diameters on VCHP performance are shown in Figure 6. For each decreasing diameter, the differences between the vapor temperature of the heat pipe and the temperatures of the vapor chamber and cold plate increased significantly. The larger diameters had the lowest temperatures; however, they also had the greatest difference in cold plate temperature as sink temperature changed. This is because a larger diameter VCHP has less vapor pressure drop and is exposed to lower heat fluxes but, since the reservoir size was held constant, the vapor to NCG mass ratio increases. Vapor pressure drop results in the temperature difference between the evaporator and condenser of the heat pipe. As a result, for the same sink temperature, the evaporator runs at a higher temperature. Higher heat fluxes naturally result in larger temperature gradients. The mass ratio between vapor and NCG determines how the NCG reacts to changes in vapor temperature. For the same amount of NCG, small amounts of vapor will result in the condenser being deactivated much quicker than larger amounts of vapor.

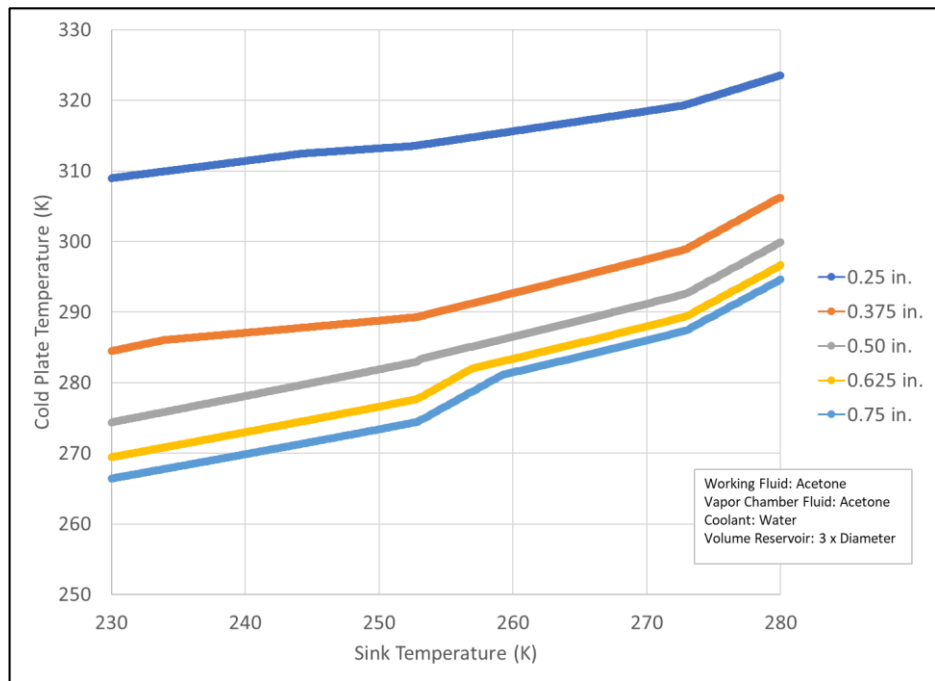


**Figure 6. Effect of Heat Pipe Diameter on VCHP Performance**

Next, the reservoir was sized based on the temperature range of interest. Since the coolant is a single-phase liquid, each VCHP will see different sink temperatures. To allow us to investigate this impact, the model was updated to include three VCHPs operating together. Results of a case study where a square reservoir was varied in size based on side length are shown in Figure 7 and Figure 8.

As seen in these figures, adjusting reservoir size has two effects. Smaller reservoirs allow the VCHP to operate at a lower temperature. This is because the reservoir reduces available condenser length which, in turn, reduces available heat transfer area. However, smaller reservoirs also do not provide as tight of temperature control. This effect results from less available non-condensable gas mass. Less mass means a larger temperature change is required for smaller reservoirs to block off the condenser compared to their larger counterparts. The trade-off for better control, however, is increased thermal resistance. In Phase I, tight temperature control is desired. For this reason, a 3 in<sup>3</sup> reservoir

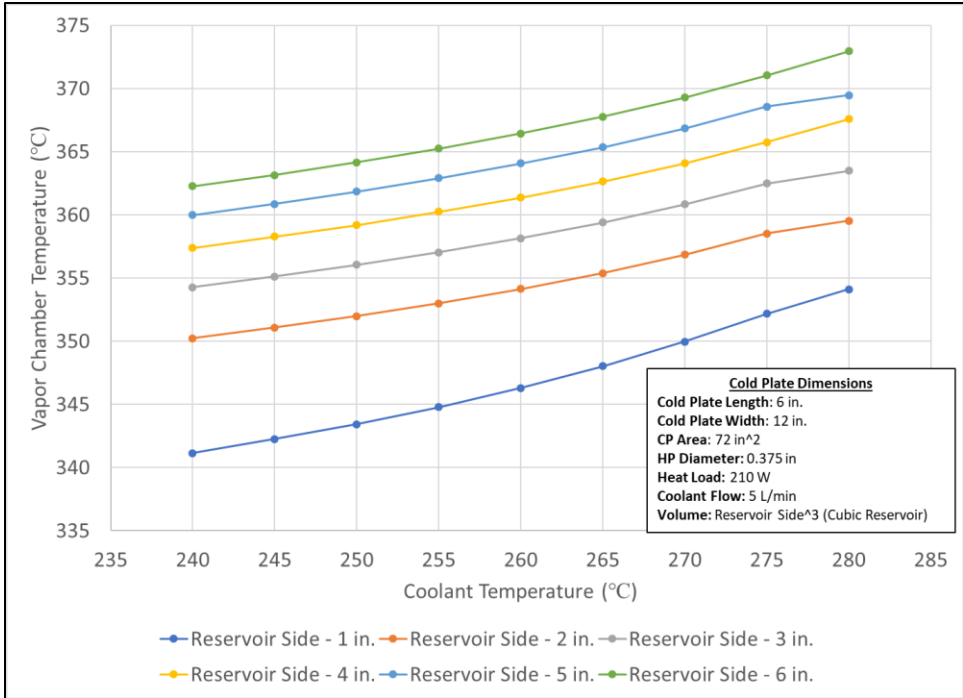


**Figure 7. Impact of Varying Reservoir Size on Vapor Chamber Surface Temperature vs. Coolant Temperature**

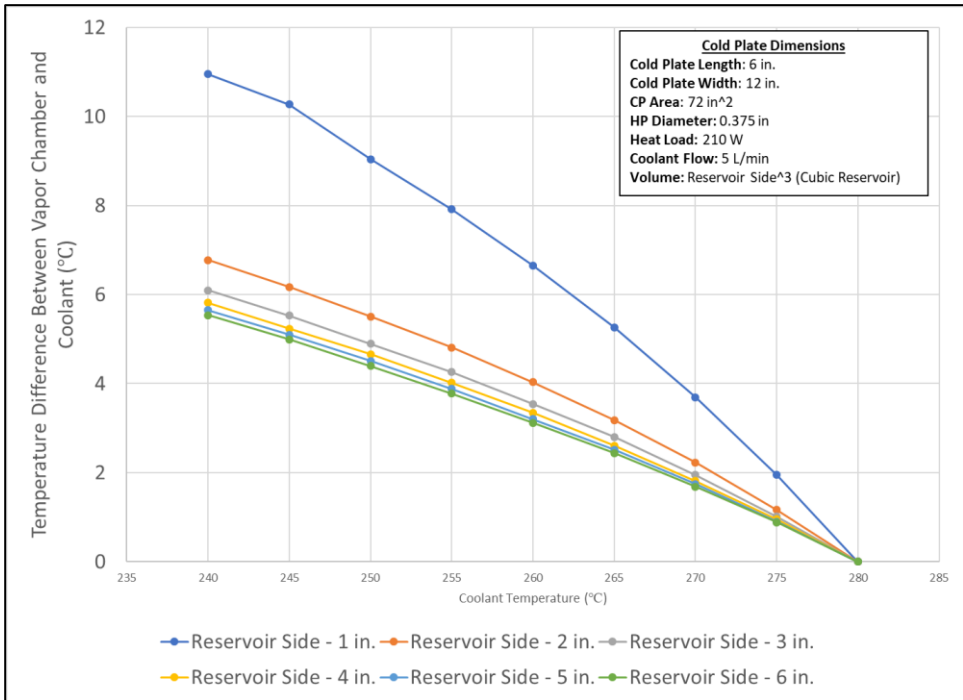


**Figure 8. Impact of Reservoir Size on Thermal Resistance vs. Coolant Temperature**

through porous media. Initially, ACT optimized for a screen-wick, but the same process can be applied to a sintered or groove wick.

$$\dot{V} = \frac{K}{\mu} \frac{A}{dx} \Delta P \quad (1)$$

volume was selected as not much improvement in temperature control results from increasing reservoir size after that. Thermal resistance, however, continues to increase significantly. Once the heat pipes were appropriately optimized, the next step in the design process was to investigate the wicks within the vapor chamber.

### C. Vapor Chamber Wick Analysis

Once the VCHPs were optimized, the next step in the process was to model and optimize the vapor chamber wicks. The limiting factor in vapor chamber performance is the capillary pumping power of the wicks to bring liquid to the heat collection surface. Fluid flow in the wicks can be modeled using the thermal-flow analogy for porous media. The governing equations for thermal conduction (Eq. 1) and porous media flow (Eq. 2) are mathematically equivalent aside from their coefficients and variables. By adjusting these coefficients, a thermal conduction FEA simulation can be used to model flow

$$\dot{Q} = k \frac{A}{dx} \Delta T \quad (2)$$

The volumetric flow rate is determined by the heat flux profile shown in Eq. 3, where  $h_{fg}$  and  $\rho$  are the latent heat of vaporization and liquid density of the working fluid, respectively. The coefficients are adjusted as the thermal conductivity,  $k_{analogy}$  becomes the wick permeability  $K$  divided by liquid viscosity  $\mu$  as shown by Eq. 4

$$\dot{V} = \frac{\dot{Q}}{h_{fg} \rho_{Ammonia}} \quad (3)$$

$$k_{analogy} = \frac{K_{wick}}{\mu_{Ammonia}} \quad (4)$$

Wick permeability  $K$  is a function (Eq. 5) of the screen-wick wire diameter ( $d_{wire}$ ) and wick porosity ( $\epsilon$ ), which is the gap between the mesh wire and is a function (Eq. 6) of the number of wire wraps ( $N_{mesh}$ ) and wire diameter.

$$K_{wick} = \frac{d_{wire}^2 \epsilon_{wick}^3}{122 * (1 - \epsilon_{wick})^2} \quad (5)$$

$$\epsilon_{wick} = 1 - \frac{1.05 * \pi * N_{mesh} * d_{wire}}{4} \quad (6)$$

Finally, the maximum available capillary pressure, which is determined from the surface tension of the fluid ( $\sigma_{acetone}$ ) and wick pore radius ( $r_c$ ) and is the highest differential pressure achievable by each mesh which is calculated through Eq. 7. Note that the pore radius was calculated using Eq. 8.

$$\Delta P_{max} = \frac{2 * \sigma_{Ammonia}}{r_c} \cos(\theta) - \rho_{Ammonia} * g * H_{chamber} \quad (7)$$

$$r_c = \frac{d_{wire} + s_{wire}}{2} \quad (8)$$

The mesh sizes and relevant parameters that were used for the FEA analysis are present in Table 2. Flow conductivity, which is the equivalent thermal conductivity for the thermal flow analogy, and the maximum capillary pressure rise is shown for each mesh number in Figure 9. The pressure rise increases linearly with mesh number as this parameter is inversely related to pore size. The flow conductivity,  $k_{analogy}$ , depends on a polynomial function of wire diameter and mesh number, so as the mesh number increases and wire diameter decreases, the wick permeability also decreases.

**Table 2. Mesh Parameters Investigated by FEA**

Mesh	$d_{wire}$ (in.)	$s_{wire}$ (in.)	$P_{max}$ (Pa)	$H_{max}$ (in.)	$k_{analogy}$ (m <sup>3</sup> s/kg)
80	0.0055	0.007	151.4	1.75	2.417E-6
120	0.004	0.0043	285.3	2.64	9.160E-7
200	0.0021	0.0029	548.4	4.38	4.176E-7

Next, the pressure drops for each of the screen-meshes was simulated using Finite Element Analysis (FEA). The heat load for the acetone subscale VCCP was assumed to be 5 W/cm<sup>2</sup> over the entire heated surface, which represents the worst-case scenario for liquid return. This equated to a 9.24x10<sup>-7</sup> m<sup>3</sup>/s equivalent flow rate at each heat pipe for the thermal flow analogy for a three-heat pipe array. The equivalent thermal conductivity is shown in Figure 9. For each mesh, the number of wraps was varied from 2 to 6 wraps, and the pressure drop was estimated accordingly. The results of this analysis are shown in Figure 10.

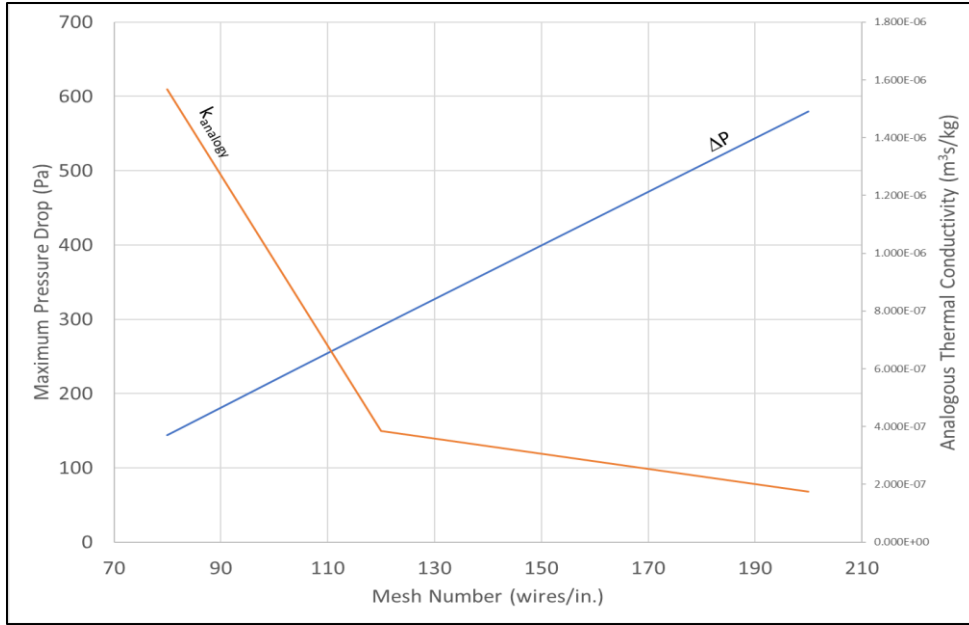


**Figure 9. Flow Conductivity and Capillary Pressure Rise for Varying Wick Number**

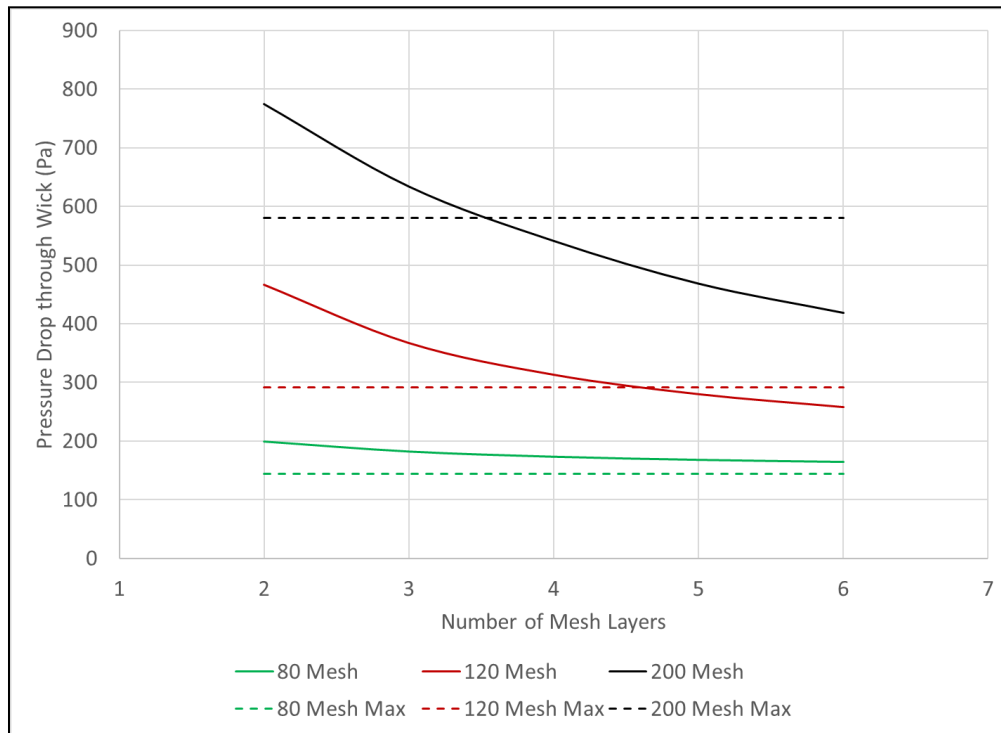


**Figure 10. Pressure Drop Results from FEA Analysis**

### III. Testing and Results

#### A. Fabricated Prototype

Using the analytical model and FEA thermal-flow analogy, ACT optimized the subscale prototype design and developed a prototype design fit for fabrication. The prototype was designed for fabrication by additive manufacturing, specifically Direct Metal Laser Sintering (DMLS) of the Aluminum alloy AlSi10Mg. This casting alloy is commonly used for DMLS parts. The evaporator and condenser were designed to be printed separately and were joined later by welding the adiabatic sections of each VCHP to these two components. Additionally, ACT welded a backplate and fill tubes to the assembly, and screen wicks to the interior of the vapor chamber and the VCHPs, as seen in Figure 11. Once fabrication was complete, the VCCP was charged with acetone in the vapor chamber, and with acetone and argon in the VCHPs.

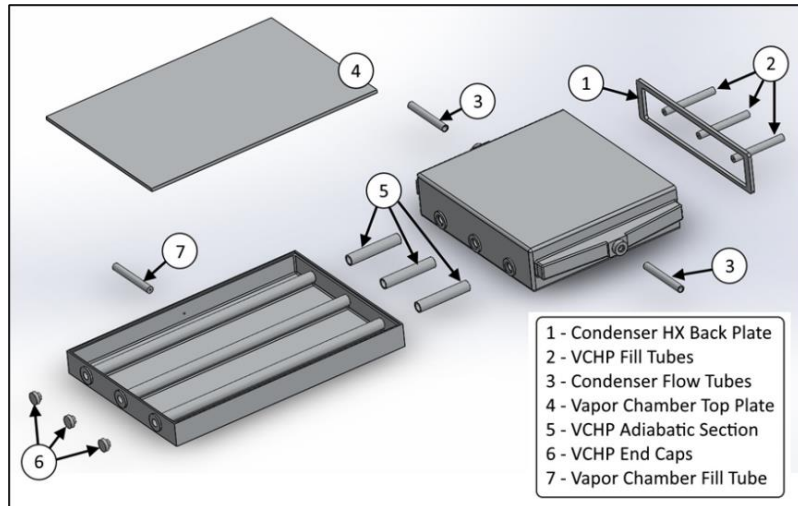


Figure 11. Exploded View of the VCCP Assembly

#### B. Test Plan

The test loop, shown in Figure 12, is relatively straightforward. An open-air accumulator was located above the pump to provide sufficient Net Positive Suction Head (NPSH). The pump drives coolant through a flow meter and then the test section. Coolant inlet and outlet temperatures are measured to allow for calorimetry. The system was charged with a 50/50 mixture of Propylene Glycol and Water. For testing, the coolant was initially kept at room temperature (approximately 20 °C) and the pump was run at approximately 2 L/min. The heaters on the heat collection surface were uniformly held at a constant power of 10 W/in<sup>2</sup> until the temperature of the surface reached steady state, at approximately 62 °C. From there, the coolant was chilled via liquid nitrogen running through a copper coil located in the accumulator. This was done at a steady rate until the coolant entering the VCCP Condenser reached -20 °C, at which point the flow of liquid nitrogen was shut off via a solenoid valve and tank heaters located within the accumulator would turn on. The test was run until coolant would once again reach room temperature of 20 °C, at which point the test was complete.

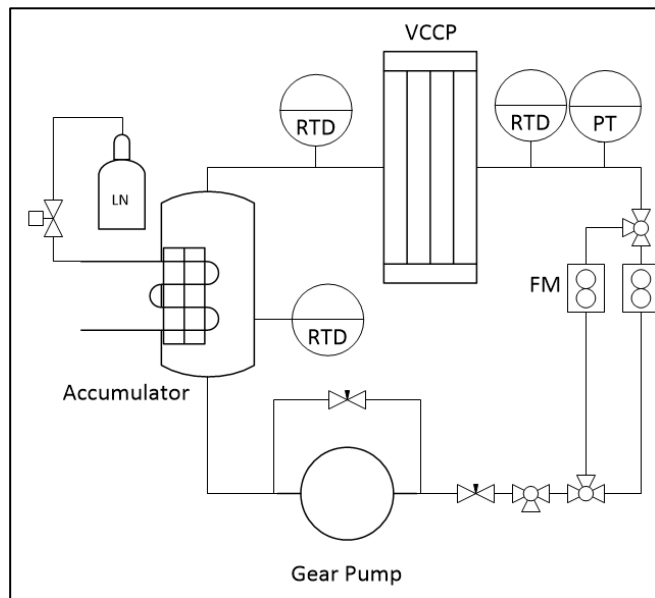


Figure 12. Test Loop

Data was collected using a Programmable Logic Controller (PLC). On the coolant side, the PLC collected measurements from the flow meter, pressure transducer, and RTDs. On the cold plate side of the system, the PLC recorded temperature measurements from 22 Thermocouples evenly distributed between the 15 heaters on the cold plate and the total power input to the heaters. In addition to data acquisition, the PLC also provided a safety shutoff for the heaters should the vapor chamber begin to overheat. This was necessary to prevent damage to the vapor chamber from overpressure. The PLC also used a PID controller to control the coolant temperature.

### C. Test Data

Figure 13 depicts the average surface temperature, and the coolant temperatures for a representative test. The temperatures recorded from the 22 thermocouples on the heat collection surface was averaged and compared to the coolant temperature across the duration of the test. As seen in this figure, there was minimal surface temperature change throughout the duration of the test, despite a 40 K sink temperature change. In the initial tests, Type T thermocouples were used and, as the temperature change was minimal, an accurate measurement of the rate of surface temperature change was not possible. In future tests, a more accurate temperature sensing method will be used.

The  $\Delta T$  across the surface was  $2^{\circ}\text{C}$  or less, which is within the range of error for the Type T thermocouples used. This can be seen in the contour plot presented in Figure 14.

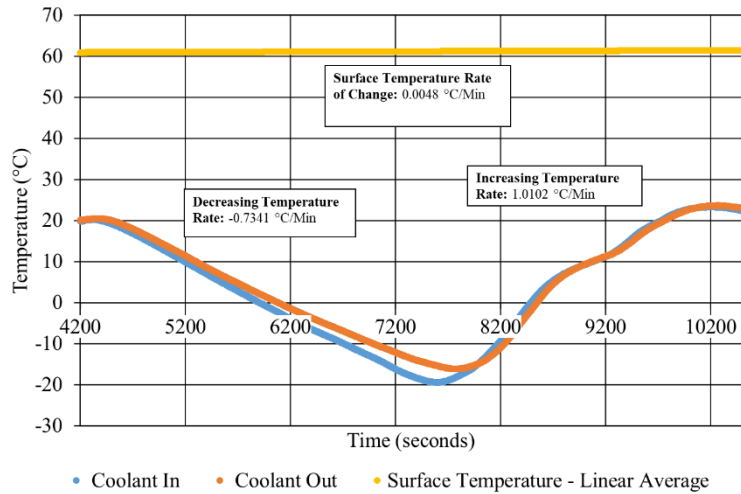


**Figure 13. A Representative Test of the Subscale Acetone VCCP**



■ 55-56 ■ 56-57 ■ 57-58 ■ 58-59 ■ 59-60 ■ 60-61 ■ 61-62 ■ 62-63 ■ 63-64 ■ 64-65

**Figure 14. Surface Chart of the Average Surface Temperature across the heat collection surface of the subscale Acetone VCCP.**

#### **IV. Conclusion**

This research was completed as part of a Phase II SBIR program. After the successful conclusion to the Phase I effort, ACT was able to demonstrate that the technology developed has the potential to meet the temperature control needs as specified by NASA. As the Phase II project is currently ongoing, there are upcoming changes to the subscale testing bed that are worth mentioning. The heaters used on the heat collection surface of the VCCP were previously controlled in parallel such that they would all turn on simultaneously, and all would produce 10 W/in<sup>2</sup> of power. The system is now being changed such that the heaters will be capable of 100 W/in<sup>2</sup> of heat load, and will be individually controlled such that a variety of arbitrary arrangements may be tested. A separate PLC is being constructed to both monitor and control the heaters. Additionally, ACT is working on the design and fabrication of another subscale prototype VCCP, albeit this time with ammonia as the working fluid. Ammonia was determined by NASA to be the preferred working fluid for spacecraft electronics cooling, and so ACT is working through the analytical model to optimize such a design.

#### **Acknowledgments**

ACT acknowledges Aryiannah McGee for her efforts in data acquisition for this research. Additionally, ACT thanks the NASA SBIR program for financially supporting the development of the technology investigated in this program. We also greatly appreciate the direction provided by our technical monitor, Jeff Didion, and his team.